Composite Structures 132 (2015) 372–383

Contents lists available at ScienceDirect

Composite Structures

journal homepage: www.elsevier.com/locate/compstruct

Experimental investigation of thermal shock effects on carbon–carbon composites

Alma L. Leanos, Pavana Prabhakar *

Department of Mechanical Engineering, University of Texas at El Paso, El Paso, TX 79968, USA

ARTICLE INFO

Article history:
Available online 27 May 2015

Keywords:
Carbon–carbon composite
Thermal shock
Mechanical properties
Compressive response
Carbon degradation

ABSTRACT

In this paper, both compressive properties and oxidation behavior of pristine and thermal shock exposed 2D C/C composite specimens were examined. Pristine test specimens were exposed to thermal shock conditions with temperatures ranging from 400 °C to 1000 °C in an oxidizing environment, followed by compression tests on pristine and thermal shock exposed specimens to obtain their compressive responses. The experimental results showed that 2D C/C composite compressive stiffness and strength decreased with increasing thermal shock temperature. Also, upon exposure to thermal shock, the stress–strain response displayed a non-linear behavior prior to failure as compared to the pristine C/C composite that failed in a brittle manner. Furthermore, it was observed by microstructural analysis that at low temperatures, i.e., 400 °C, the oxidation attack was uniform through the interior of the composite. On the other hand, at moderate temperatures, i.e., 600 °C, oxidation occurred rigorously at the surface of the composite. At high temperatures, i.e., above 600 °C, the specimens experienced the two aforementioned oxidation mechanisms. Therefore, it was concluded that carbon matrix degraded rapidly when exposed to thermal shock conditions in oxidizing environments and protective coating is required to maintain the quality of the composite under such conditions.

1. Introduction

Carbon fiber reinforced carbon matrix composites, called carbon–carbon (C/C) composites retain exceptional thermal and mechanical properties such as high modulus, high thermal shock resistance and high specific strength at high temperatures in non-oxidizing environments. C/C composites have demonstrated to be very promising candidates to be used as structural components in many defense applications, like navy and aerospace structures. However, most of these components are exposed to thermal shock conditions in oxidizing environments with temperatures above 450 °C, under which carbon constituents burn away rapidly [1]. Zhao et al. [2] have demonstrated that oxidation has a strong effect on the C/C composite mechanical properties, nevertheless, limited studies have been conducted to analyze the properties and microstructure of unprotected C/C composites under thermal shock conditions in oxidizing environments [1–3]. Manocha [1] states that when C/C composites are exposed to high temperature tests in oxidizing environments, their properties degrade around 10 to 20% depending on the temperature and time under which they are exposed. Similarly, numerous studies have investigated the tensile and flexural strength of C/C composites at high temperatures [4–10], but there is seldom information available about through-thickness compressive properties of 2D C/C composites after being exposed to thermal shock conditions. Therefore, there is a great interest in analyzing the effects of oxidation on the properties and microstructure of C/C composites in order to assure their good performance in high temperature structural applications.

With the increasing thickness of laminates used in naval and aerospace structures, primarily for ballistic applications, understanding the influence of through-thickness and lateral impact loads on the mechanical response and failure has become very critical [11–13]. Lateral loads often result in delamination type failure due to the presence of weak interfaces. Though these delaminations may not cause catastrophic failure of structures, they jeopardize the structural integrity by reducing their resistance to buckling failure. Therefore, the purpose of this work is to investigate the through-thickness compressive properties of 2D woven C/C composites when exposed to thermal shock conditions in an oxidizing environment.

An overview of the experimental procedure followed in the present study is shown in Fig. 1. First, pristine C/C composite specimens were thermally exposed to five different thermal shock

* Corresponding author. Tel.: +1 915 747 5863.
E-mail address: pprabhakar@utep.edu (P. Prabhakar).

http://dx.doi.org/10.1016/j.compstruct.2015.05.038
0263-8223/

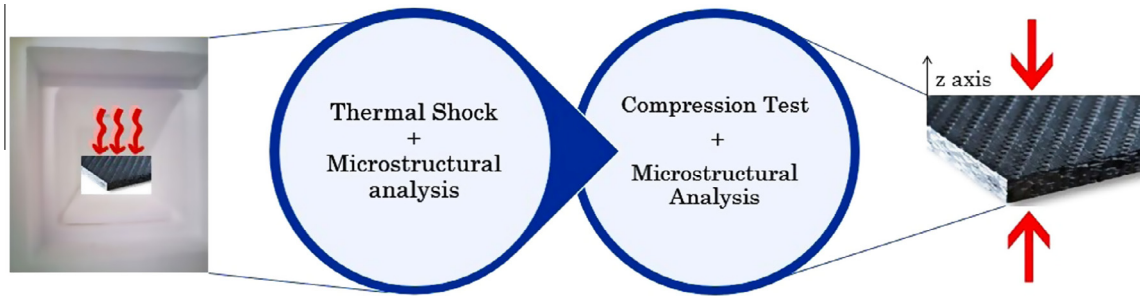

Fig. 1. Schematic representation of experimental procedure.

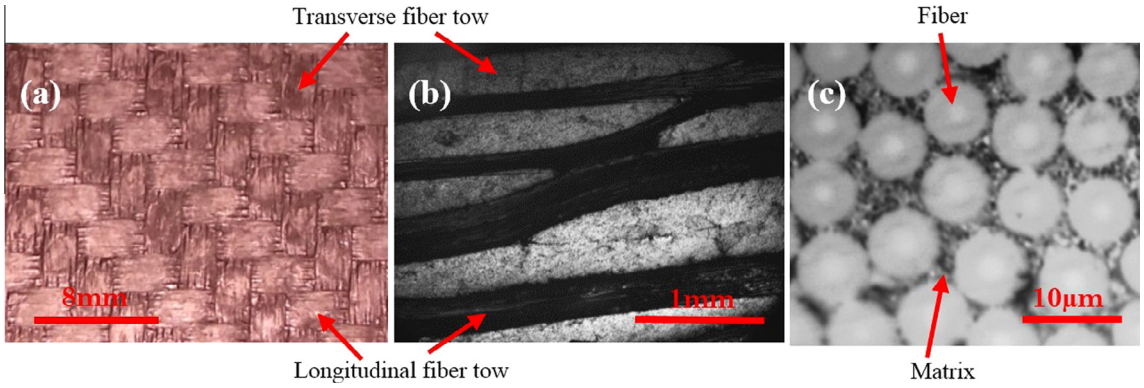

Fig. 2. Optical Micrograph of 2D C/C Composite (a) top surface (b) cross-section and (c) magnified cross-section.

conditions, each with peak temperature of 400 °C, 600 °C, 700 °C, 800 °C and 1000 °C, respectively. Then, through-thickness compression tests were conducted to determine the compressive stiffness and strength of pristine and exposed C/C composite specimens. Finally, a microstructural analysis of C/C composite specimens exposed to different thermal shock conditions was carried out to analyze the carbon morphology due to oxidation. Similarly, the microstructure of the C/C composite was analyzed after each compression test to identify possible modes of failure.

2. C/C Composite oxidation

Several previous research efforts have been made to understand the oxidation kinetics of unprotected C/C composites [14–19]. However, the oxidation behavior of C/C composites varies depending on the desired weave geometry, type of carbon materials, microstructure and processing condition [2,20]. Luthra [21] summarizes the oxidation behavior of unprotected C/C composites with three main stages. First, oxidizing gas (e.g., O_2) starts diffusing across the boundary layer at the surface of the composite. Following this, oxygen can either react chemically with carbon materials located at the surface of the composite, producing gases in form of CO and CO_2, or oxygen can diffuse through existing cracks in the composite. Luthra [21] states that at low temperatures, gas diffusion is the main mode of oxidation, whereas at high temperatures, both chemical reaction and diffusion of gaseous species through cracks in the composite control the oxidation process. At this stage, oxidation attack occurs at the surface and within the interior of the composite.

In addition to this, fiber/matrix interface along the fiber tows possesses preferential oxidation due a mismatch of coefficient of thermal expansion between the matrix and fiber, as explained by Crocker and McEnaney [15]. Also, the fiber edges are more sensitive to oxidize than the center or bulk of the fibers, creating a pointed morphology at the exposed ends of the fibers [17,18,22].

Moreover, Bacos [3] affirms that for 2D C/C composites, carbon matrix degradation prevails during an oxidation process, since the reactivity of the carbon matrix is higher than that of the carbon fibers. This author also states that at low temperatures, oxidation damage is distributed uniformly throughout the interior of the composite and swollen cracks/voids are observed more frequently in the tows due to gaseous species transport. This oxidation behavior usually leads to the propagation of consumed channels along the fiber tows. On the other hand, at high temperatures, Bacos [3] declares that only the first layers of the composite are extensively oxidized, while the fiber tows and matrix within the exposed surfaces show minimal evidence of oxidation.

3. C/C Composite compressive response

Though there are no ASTM standards available to perform through-thickness compression tests on 2D fiber-reinforced composites [23,24], through-thickness compressive stiffness of fiber-reinforced composites has been measured by Lodeiro et al. [25]. Difficulties faced during determining the compressive strength of 2D fiber-reinforced composites are reported in the literature. For instance, high stresses develop at the ends of the specimens during compression test [25], strength is sensitive to changes in the cross-sectional area [26], friction within the loading plates and the specimen affects the strength values [27], strain measurements from crosshead displacements and strain gauges provide different strength results [23] and the strength is easily affected by the specimen geometry [27], among others. Conversely, Hodgkinson [28] affirms the feasibility of testing

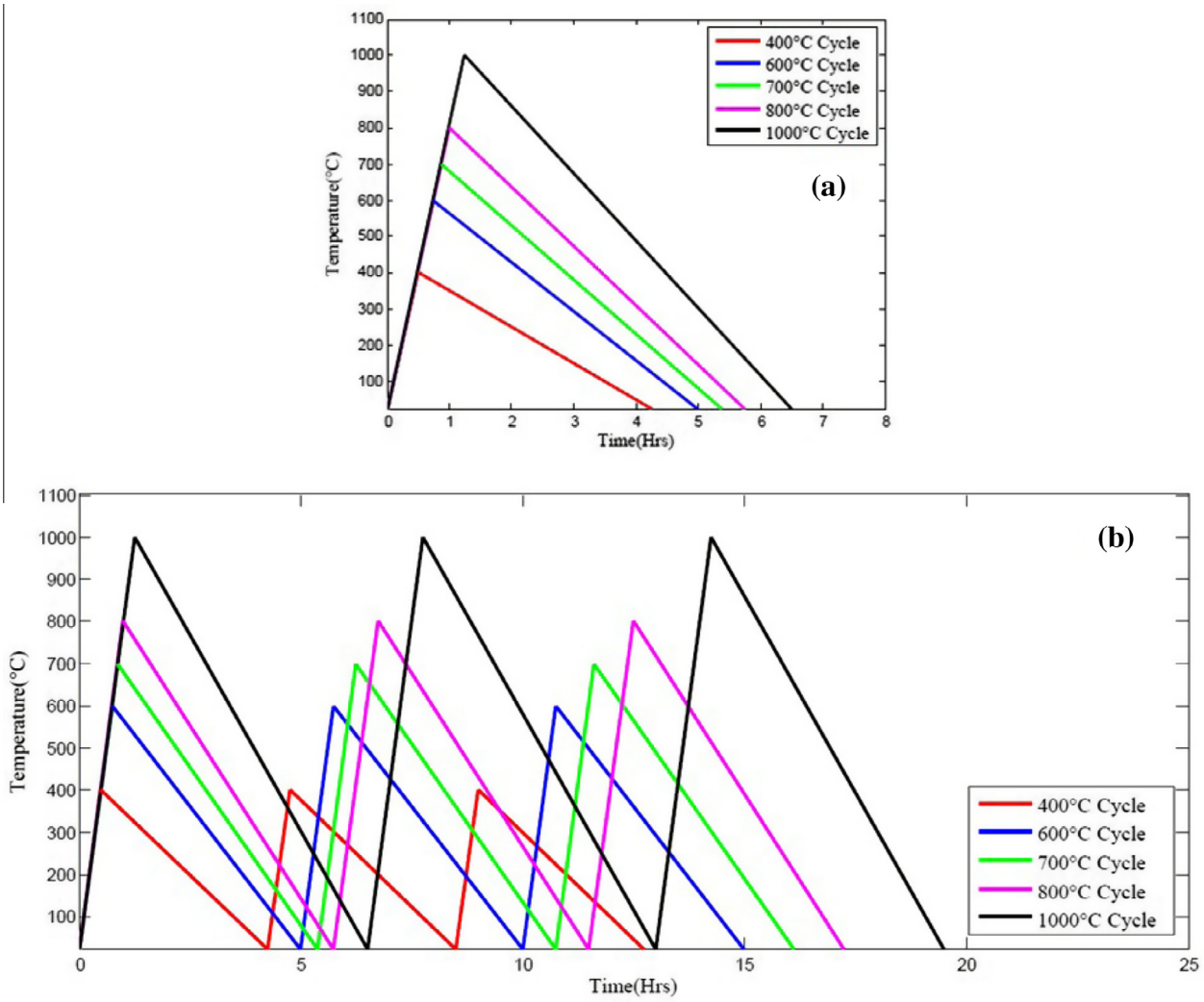

Fig. 3. Schematic representation of the five different thermal shock conditions (a) one cycle and (b) three cycles. Peak temperatures have a tolerance of ±2 °C, heating rate is 12.5 ± 2 °C/min and cooling rate varies from 3 ± 0.5 °C/min to 1.6 ± 0.5 °C/min.

unidirectional carbon/epoxy square specimens with a minimum thickness of 6 mm to determine through-thickness compressive stiffness.

Furthermore, there is seldom information available regarding the failure analysis of 2D C/C composite specimens under compressive loads. Park and Lee [29] observed two modes of failure in carbon-phenolic woven materials, i.e., horizontal and angular splitting of layers within the laminate. They suggest that during compression tests, matrix cracks propagate through the thickness of the composite leading to fiber breakage and consequently, complete failure.

4. Experimental procedure

4.1. Specimen Description

In the present work, a 2D woven C/C composite (supplied by Bay Composites, Inc., USA) was investigated. This composite consists of 6000 polyacrilonitrile (PAN) carbon fibers arranged in longitudinal and transverse tows, which are interwoven following a 2 × 2 direct twill weave pattern to create a single lamina, as shown in Fig. 2. The composite was made of 10 of such plies, vacuum densified with phenolic resin as matrix precursor and exposed to a final heat treatment temperature of 1100 °C.

The C/C composite plate, with average thickness of 0.2067 ± 0.01 inches, was sectioned into square specimens with sides of 0.5 ± 0.05 inches (by caliper measurements) using a wet tile saw with a diamond blade. These specimens were grouped according to the thermal shock condition at which they were exposed, and they will be called **test specimens** throughout this study. Test specimens were hand-abraded using 240, 400, 600, 800 and 1200 grit SiC papers, followed by 6 μm and 1 μm diamond abrasives on TEXPAN and ATLANTIS polishing pads, respectively. Finally, the test specimens were polished with 0.05 μm alumina on NAPPAD polishing pad for a perfect finish (all supplied by Pace Technologies, USA). The microstructure of the test specimens was captured using an optical microscope (Model NJF-120A, OMAX Corporation, USA) and a variable-pressure table-top scanning electron microscope (Model TM1100 SEM, Hitachi High Technologies America, Inc., USA). Specimen preparation was performed at room temperature and 1 atmosphere air pressure.

4.2. Thermal shock conditions

Pristine test specimens were heated using a heating furnace (Model BF51766A-1 Lindberg/Blue M, Thermo Fisher Scientific, Inc., USA). Test specimens were placed in a ceramic boat inside the furnace and heated from room temperature (25 ± 5 °C) to the

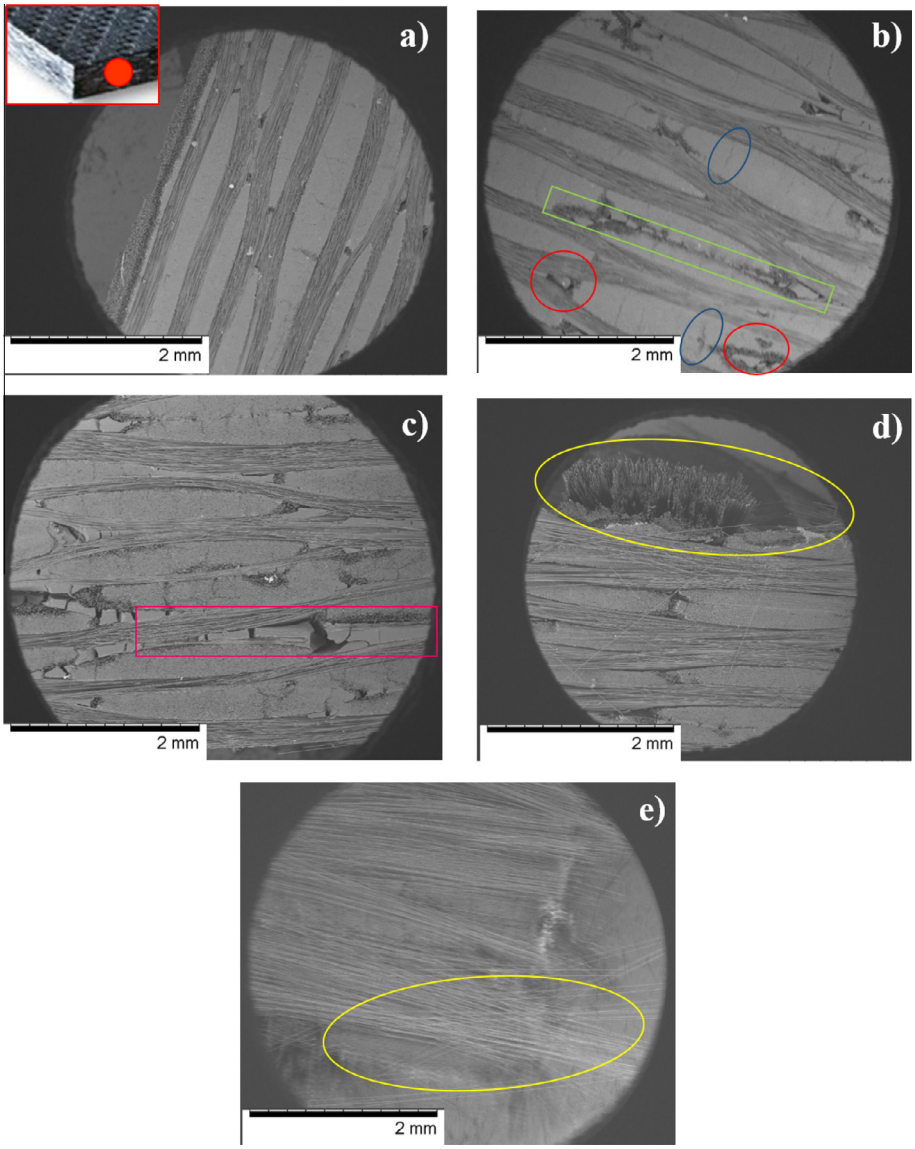

Fig. 4. SEM micrograph of (a) Pristine (b) 400 °C (c) 600 °C (d) 700 °C and (e) 800 °C 2D C/C composite test specimens (1 cycle). Void growth is shown in red, transverse crack propagation in blue, tow/matrix interface degradation in green, matrix macroscopic cracking in pink and surface degradation in Yellow. (For interpretation of the references to colour in this figure legend, the reader is referred to the web version of this article.)

desired thermal shock temperature at a constant heating rate of 12.5 ± 2 °C/min. Peak temperatures were reached with a tolerance of ± 2 °C and the cooling rate ranged from 3 ± 0.5 °C/min for 400 °C cycle to 1.6 ± 0.5 °C/min for 1000 °C cycle. The cooling rate of the machine was dependent on the peak temperature achieved, and therefore, was solely a limitation of the machine. That is, the total time for an experiment with a peak temperature of 1000 °C to cool down to room temperature was higher as compared to the one with a peak temperature of 400 °C. Fig. 3(a) and (b) show a constant heating rate up to the peak thermal shock temperatures, while the cooling rate was minimum for the 1000 °C cycle.

First, five pristine specimens were exposed to five thermal shock conditions (one cycle), with temperatures of 400 °C, 600 °C, 700 °C, 800 °C and 1000 °C, respectively, as shown in Fig. 3(a). Thermal shock experiments were performed at room temperature in steady air and 1 atmosphere air pressure. The microstructure of these five thermal shock exposed test specimens was captured before the compression tests (described in the next section) using the optical microscope and the SEM. Then, five test specimens were exposed to each of the temperatures aforementioned, according to the thermal shock conditions shown in Fig. 3(b) for three cycles. The experimental conditions of the three cycle tests were the same as those for one cycle thermal shock experiments. The microstructure of these test specimens was analyzed before the compression tests, as explained previously, however, since the observed composite oxidation morphology was very similar to that observed on one cycle thermal shock test specimens, an additional test specimen was added to each thermal shock condition (three cycles) in order to analyze the microstructure under the exposed surface. For this purpose only, test specimens were mounted in epoxy, polished and examined using the optical microscope and the SEM.

4.3. Compression tests

Five pristine specimens were exposed to through-thickness compression loading to determine the pristine compressive stiffness and strength. Besides this, compression tests were performed

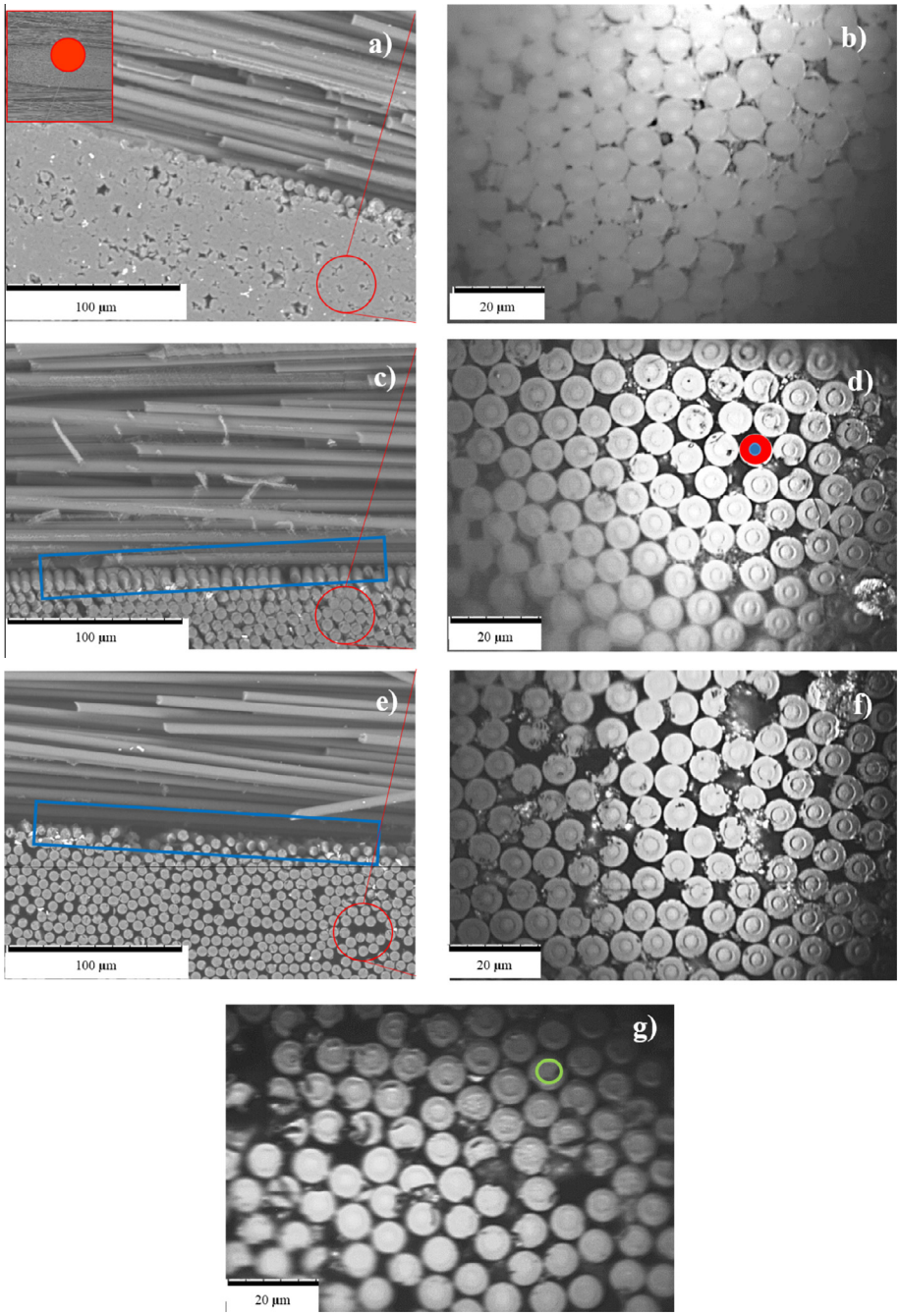

Fig. 5. SEM micrograph showing tow/matrix interface of (a) Pristine (c) 600 °C and (e) 700 °C; Optical micrograph showing enlarged images of fibers within a tow of (b) Pristine (d) 600 °C (f) 700 °C and (g) 1000 °C 2D C/C composite test specimens (1 cycle). Tow/matrix degradation is shown in blue, fiber edge in red, fiber core in blue and core diameter in green. (For interpretation of the references to colour in this figure legend, the reader is referred to the web version of this article.)

on one test specimen for each thermal shock condition (one cycle) and on five test specimens exposed to each of the three cycles thermal shock condition. Next, the measured compressive properties were compared with those of the pristine specimens. The stress–strain responses of the pristine and exposed test specimens are shown in the results section. All compression tests discussed in this study were performed at room temperature in steady air and 1 atmosphere air pressure using a servohydraulic fatigue testing system (Model 8801, Instron Corporation, USA).

The 2D C/C composite compressive properties, i.e., stiffness and strength, were determined by applying compressive load in the through-thickness direction of the specimens using a rectangular stainless steel fixture with a plate of the same material used to support the specimen during compression. The actuator speed of the testing machine was 1 mm/min and the stress was defined as the force applied through-thickness direction of the composite over the area of the top surface of each specimen (obtained by caliper measurements). Likewise, the strain was determined from the displacements provided by the crosshead movements with respect to the original average thickness of the composite. Finally, one of the five failed test specimens (previously exposed to three cycles of thermal shock conditions) was mounted in epoxy, polished

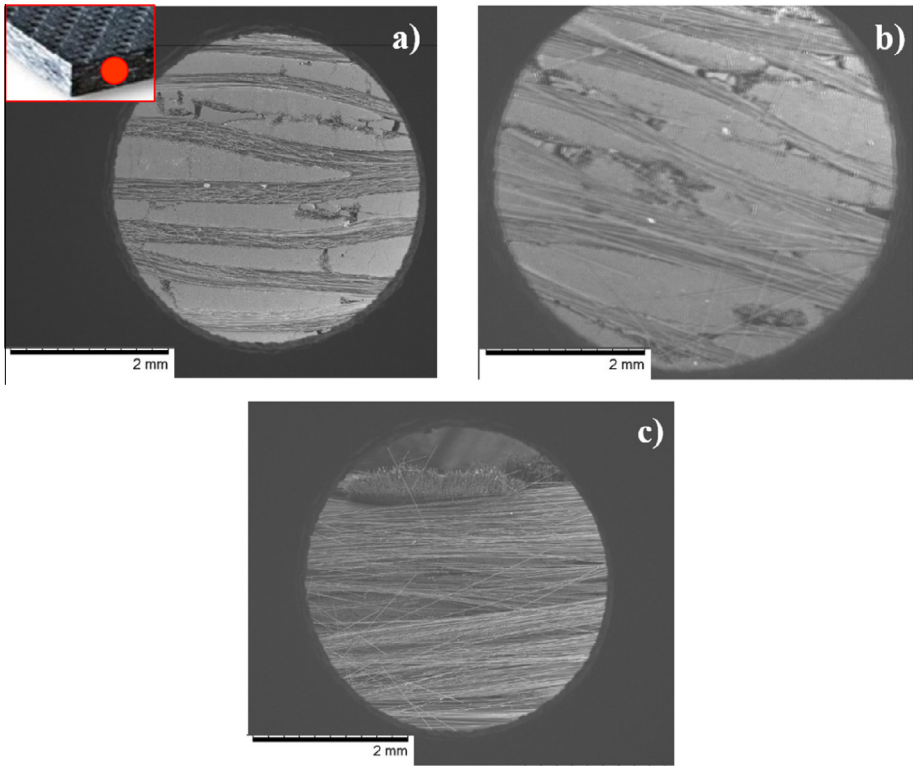

Fig. 6. SEM micrograph of (a) 400 °C (b) 600 °C and (c) 700 °C 2D C/C composite test specimens (3 cycles) showing surface oxidation.

Fig. 7. 1000 °C 2D C/C composite test specimen (3 cycles) showing fibers separating from the surface.

and examined using the optical microscope and the SEM to capture possible modes of failure.

5. Results

5.1. Microstructure analysis after thermal shock conditions

The microstructure of one of the lateral surfaces of the test specimens exposed to one cycle and three cycles of thermal shock was analyzed for each peak temperature, followed by the analysis of the top surface of test specimens exposed to one cycle thermal shock condition. Further, test specimens exposed to three cycles of thermal shock were polished in order to analyze the structure within the interior of the composite. All these microstructural analyses together provided reliable predictions of the corresponding modes of oxidation.

Microstructural examination of test specimens exposed to one cycle thermal shock condition is shown in Fig. 4 for different peak temperatures. At 400 °C, oxidation mechanisms as void growth (shown in red in Fig. 4 (b)) and transverse crack growth (shown in blue in Fig. 4(b)) were observed in the exposed surface, suggesting that oxidizing gas was trying to diffuse through existing cracks/voids located at the lateral surfaces of the test specimens. Likewise, the tow/matrix interface started decomposing at 400 °C (transverse view of degradation shown in green in Fig. 4(b)), resembling the initiation of consumed longitudinal channels that are usually created during an oxidation process. Similar oxidation behavior was observed for test specimens exposed to 600 °C, however, the tow/matrix interface seemed to be extensively oxidized as macroscopic cracks were developed in the matrix surrounding the tows (shown in red in Fig. 4(c). This type of material degradation suggests that oxidation attack was concentrated on the exposed surfaces of the test specimens. Finally, at higher temperatures, i.e., above 600 °C, both the carbon matrix degradation at the surface and the amount of fibers protruded from the surface increased with increasing thermal shock peak temperature, as shown in yellow in Fig. 4(d) and (e) for 700 °C and 800 °C test specimens, respectively.

Interface between the longitudinal and transverse fiber tows of pristine specimen and specimens exposed to one cycle thermal shock condition are shown in Fig. 5(a), (c) and (e), whereas Fig. 5 (b), (d), (f) and (g) show the magnified images of transverse fibers within a tow. Fig. 5(a) shows the undamaged tow/matrix interface and Fig. 5(b) demonstrates that the non-oxidized fibers within a tow are well packed together by the surrounding carbon matrix. It is observed that the tow/matrix interface degradation increased with increasing thermal shock peak temperature, as shown in blue in Fig. 5(c) and (e) for 600 °C and 700 °C test specimens, respectively. Similar image for the 400 °C test specimen is not shown as the tow/matrix interface degradation was minimal. Furthermore, as stated earlier, the carbon matrix degraded rapidly with increasing thermal shock peak temperature from 600 °C to 1000 °C, leaving gaps between fibers, as shown in Fig. 5(d), (f) and (g).

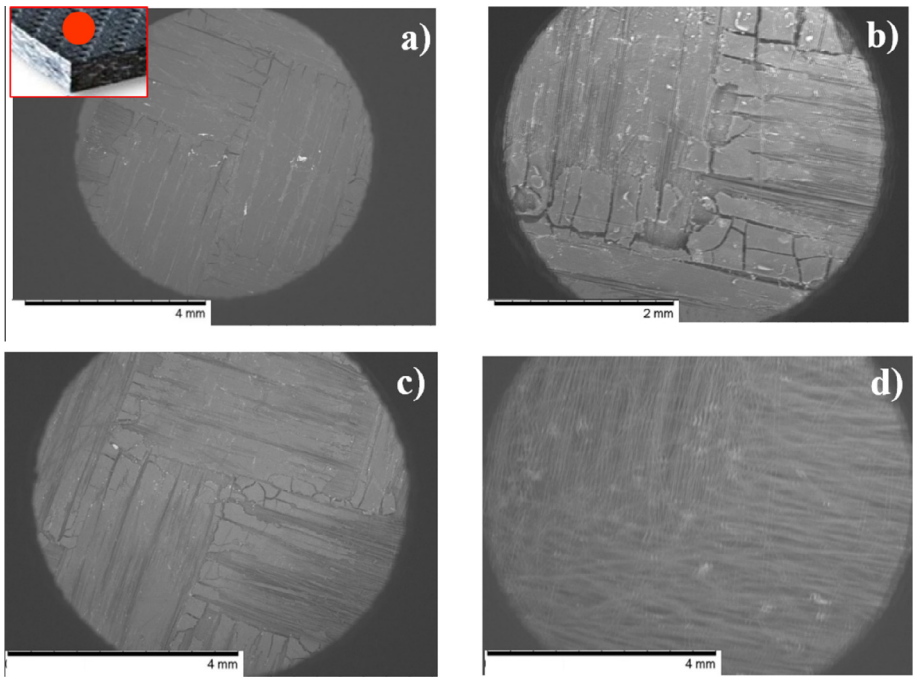

Fig. 8. SEM micrograph of top surface of (a) pristine (b) 600 °C (c) 700 °C and (d) 800 °C 2D C/C composite test specimens (1 cycle) showing matrix cracking and degradation.

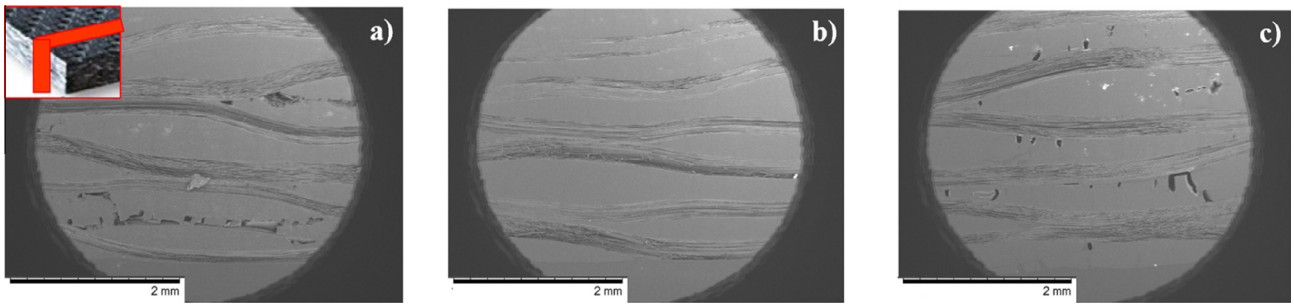

Fig. 9. Microstructural analysis of the interior of polished 2D C/C composite test specimens at (a) 400 °C (b) 600 °C and (c) 700 °C (3 cycles).

Therefore, oxidation attack for these test specimens was predominantly found on the exposed surfaces, where the ends of the fibers displayed a pointed morphology as the fiber core (blue circle in Fig. 5(d)) is known to be more resistant to oxidation than the fiber edge (red circle in Fig. 5(d)), as suggested by Han et al. [17], Glime and Cawley [18] and Lamouroux et al. [22]. It is important to notice that 1000 °C test specimen manifested the maximal surface oxidation attack, resulting in the rupture of the denuded ends of the fibers. Consequently, an increase of undamaged fiber core diameter (green circle in Fig. 5(g)) supported this oxidation behavior, which was observed previously by Han et al. [17] in oxidized 3D C/C composites.

Test specimens exposed to three cycles of thermal shock at different peak temperatures are shown in Fig. 6(a) to (c). It can be noticed that further oxidation occurred at the exposed lateral surfaces of the composite with increasing number of thermal cycles. For instance, further oxidation at the lateral surfaces of test specimens exposed to 400 °C and 600 °C resulted in a reduction of visible voids and cracks, as shown in Fig. 6(a) and (b). Nevertheless, the carbon matrix at the surface degraded further by increasing the number of thermal cycles that resulted in the fibers to separate from the surface, as shown in Fig. 6(c) for 700 °C and Fig. 7 for 1000 °C test specimens (3 cycles).

The top surface of test specimens exposed to one cycle thermal shock conditions were next analyzed (Fig. 8) to identify surface damage due to material degradation. It was observed that at moderate temperatures, i.e., above 600 °C, carbon located at the surface of the test specimens started oxidizing as the carbon matrix is more susceptible to react with oxygen than the carbon fibers. Matrix cracking and degradation at the surface of the composite increased with increasing the thermal shock peak temperature from 600 °C to 800 °C, as shown in Fig. 8(b) to (d).

Finally, microstructural analyses at both the interior and the edges right under the exposed surfaces of test specimens exposed to three cycles of thermal shock were performed. Micrographs of polished test specimens displayed more prominent modes of oxidation. By analyzing the interior of test specimens exposed to 400 °C and 700 °C, the evolution of cracks and voids through the interior of the composite was captured as shown in Fig. 9(a) and (c), respectively. On the contrary, fiber tows and matrix within the interior of test specimens exposed to 600 °C showed lesser oxidation (see Fig. 9(b)). Following this, the edge of polished test specimens was analyzed by using both, SEM and optical microscope. That is, both micrographs were taken at the same position and they were compared in order to capture most of the oxidation phenomena. It was observed that by increasing the thermal shock peak

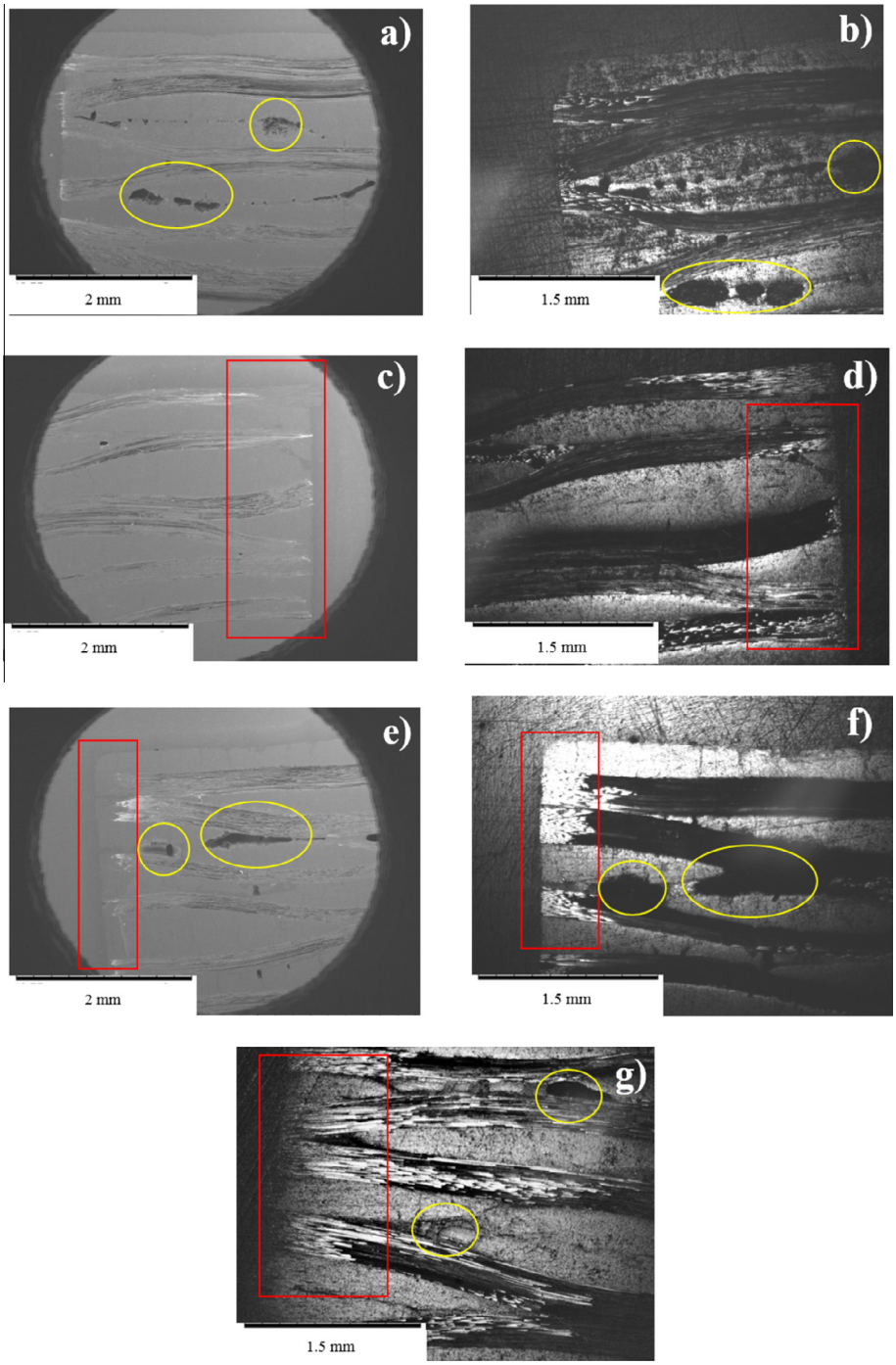

Fig. 10. SEM micrograph showing the edge of (a) 400 °C (c) 600 °C and (e) 700 °C; optical micrograph showing same edge of (b) 400 °C (d) 600 °C (f) 700 °C and (g) 1000 °C 2D C/C composite test specimens (3 cycle). Exposed fiber oxidation shown in red and void growth in yellow. (For interpretation of the references to colour in this figure legend, the reader is referred to the web version of this article.)

temperature, exposed fibers became more glossy and sharp (shown in red in Fig. 10(c) to (g)) as compared to the 400 °C test specimen (shown in Fig. 10(a) and (b)). Therefore, it was verified that oxidation attack was maximal for 1000 °C test specimen since oxidized fibers were excessively misaligned from the tow direction. Also, this behavior corroborates the observation that during the oxidation process the ends of the fibers adopt a "needle-shape", as discussed before. Further, void/crack growth was manifested for 400 °C, 700 °C and 1000 °C test specimens, as shown in yellow in Fig. 10(a), (b), (e), (f) and (g).

Therefore, microstructural examination on test specimens exposed to one cycle and three cycles of thermal shock provided evidence to state that the matrix was more susceptible to degrade than the fibers due its high reactivity. Also, the initiation of significant tow/matrix interface degradation was observed at moderate temperatures (i.e., 600 °C). The microstructural analysis also revealed that at low temperatures, i.e. 400 °C, uniform oxidation attack occurs within the interior of the composite, resulting in good agreement with Bacos [3]. At moderate temperatures, i.e., 600 °C, oxidation attack was strictly located at the surface of the

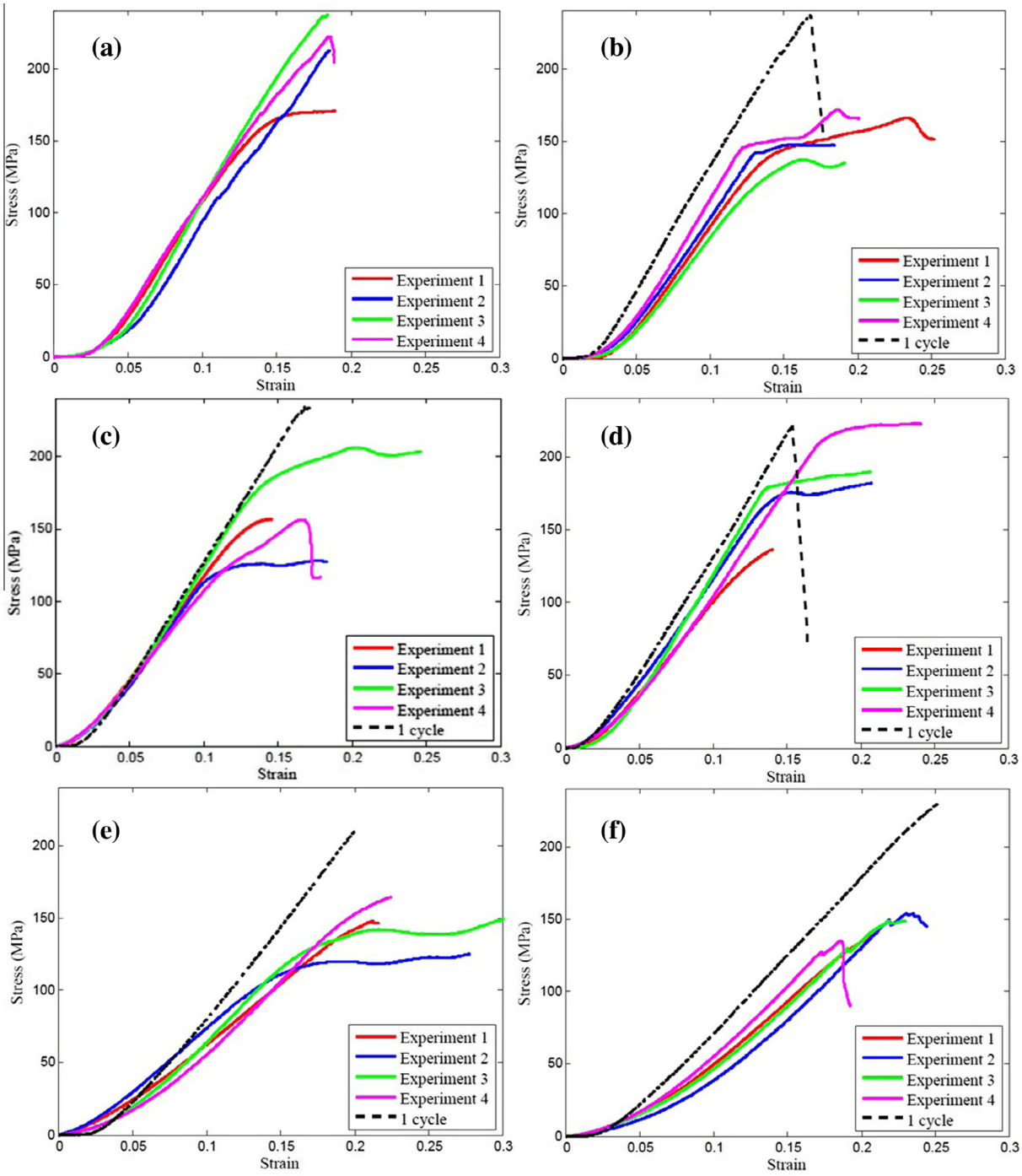

Fig. 11. Stress–strain responses of (a) pristine (b) 400 °C (c) 600 °C (d) 700 °C (e) 800 °C and (f) 1000 °C 2D C/C composite test specimens (1 and 3 cycles).

composite, while the diffusion of gases through the composite was minimal. Thus, it is suggested that chemical reaction was the main mode of oxidation for moderate temperatures. On the contrary, at high temperatures, i.e., above 600 °C, two oxidation mechanisms were present: First, oxygen reacted with carbon at the surface of the composite, followed by the diffusion of gases through the interior of the composite.

5.2. Compressive stiffness and strength

Following the experimental procedure explained previously, stress–strain responses for pristine (Fig. 11(a)) and thermal shock exposed specimens were obtained. Stress–strain responses of test specimens exposed to one and three cycles of thermal shock configurations (from 400 °C to 1000 °C) are shown in Fig. 11(b) to (f). It was verified that the compressive stiffness was lower for three cycle thermal shock conditions as compared to one cycle. The average compressive stiffness and strength of pristine 2D C/C composite specimens were determined to be 1.7 ± 0.14 GPa and 140 ± 15 MPa, respectively. The strength values were obtained from the stress–strain responses, at a point where the composite started displaying damage induced non-linearity. Through-thickness stress–strain responses of pristine specimens displayed a brittle type of failure, as shown in Fig. 11(a). Similar

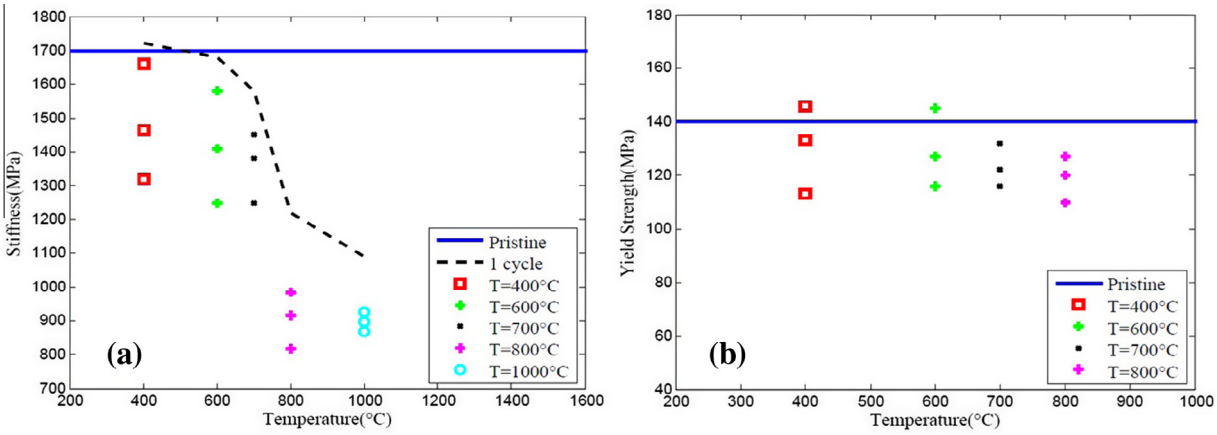

Fig. 12. Comparison of compressive (a) stiffness and (b) yield strength between pristine and exposed 2D C/C composite specimens (1 and 3 cycles).

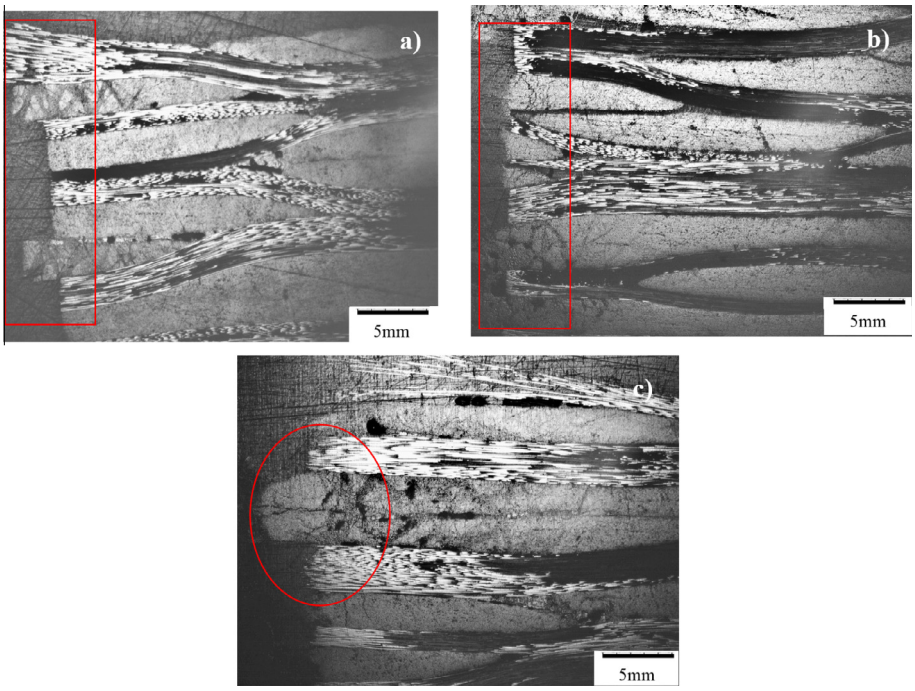

Fig. 13. Optical micrograph of (a) 400 °C (b) 600 °C and (c) 800 °C polished 2D C/C composite test specimens (3 cycles) after compression test.

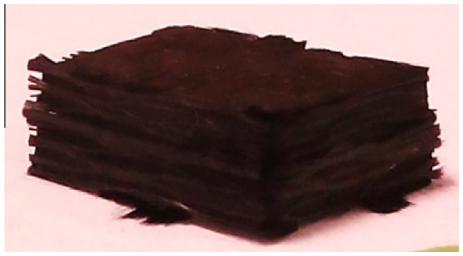

Fig. 14. 700 °C 2D C/C composite test specimen after compression test showing shear mode of failure.

behavior was found in the responses of test specimens exposed to one cycle of thermal shock, which are shown by a dashed line in Fig. 11(b) to (f).

The compressive stiffness and damage induced non-linearity for all cases, i.e., pristine, 1 cycle exposure and 3 cycle exposure are summarized in Fig. 12(a) and (b) respectively. Fig. 12(a) provides a good comparison of stiffness reduction with increasing thermal shock peak temperature, which was obtained by focusing at the initial slopes of the stress–strain responses. Likewise, damage induced non-linearity was observed in the compressive response of test specimens exposed to three cycles of thermal shock, showing a decrease in the average onset strength with increasing thermal shock peak temperature (as shown in Fig. 11(b) to (f)). These average strength values are summarized in Fig. 12 (b) showing a good agreement between repeated tests.

5.3. Microstructure Analysis After Compression Test

Microstructural analyses of test specimens subjected to compression tests after being exposed to three cycles of thermal shock were performed. The edge and the interior right under the exposed surfaces of the test specimens were studied by optical micrographs and SEM images, respectively. The examination of the edge of test

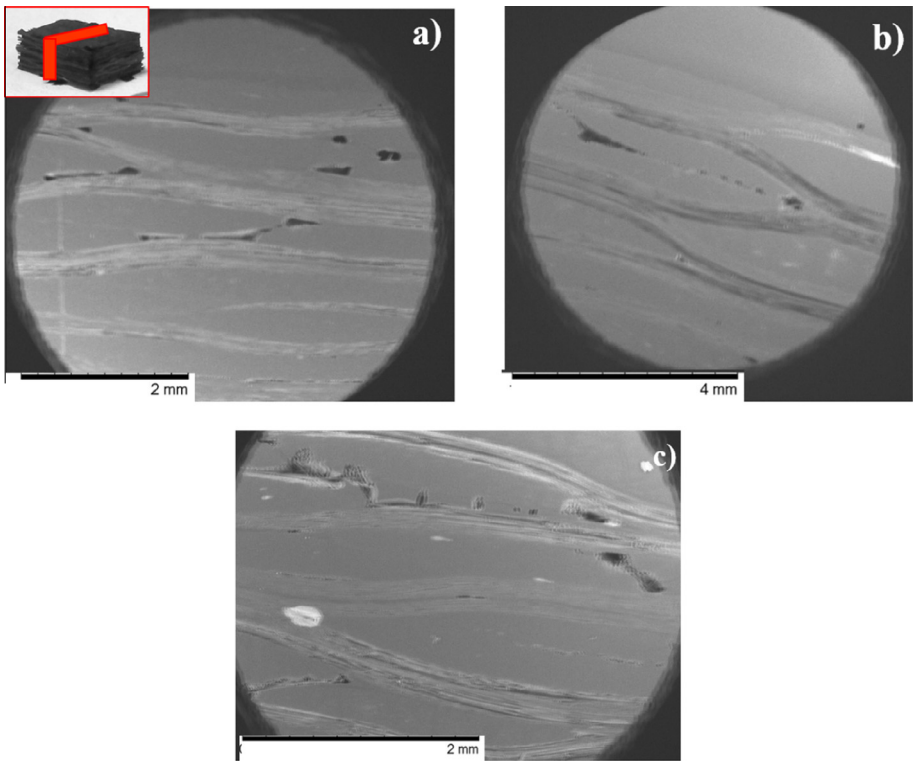

Fig. 15. SEM micrograph of (a) pristine (b) 400 °C and (c) 700 °C polished 2D C/C composite test specimens (3 cycles) after compression test.

specimens showed that fracture occurred by shear type failure between plies that run perpendicular to the applied load (weak regions), as shown in red in Fig. 13(a) to (c) and Fig. 14. Also, as explained by Bacos [3], matrix oxidation led to crack/void growth and tow/matrix degradation within the interior of the composite resulting in matrix/tow debonding that highly influenced the compressive mechanical response of the composite. Therefore, these oxidation mechanisms supported the propagation of matrix cracks, tow/matrix debonding and/or fiber tow breakage within the composite under lateral compression, causing the complete failure of the composite (as displayed in Fig. 15(a) to (c)). Pristine and 400 °C test specimens followed a brittle type failure and shear banding occurred within the first layers of the composite (as shown in Fig. 15(a) and (b)), whereas test specimens exposed to high temperatures, i.e., greater than 700 °C, followed a compliant failure as the aforementioned oxidation mechanisms supported the creation of multiple shear banding zones through the thickness of the composite (as shown in Fig. 15(c)). This latter behavior is attributed to damage induced non-linearity prior to the complete failure of the composite.

6. Concluding remarks

Through-thickness compressive properties and oxidation behavior of 2D C/C composites were determined in this study. Microstructural analyses of thermal shock exposed test specimens displayed that at low thermal shock temperatures (i.e., 400 °C), oxidation attack was observed by crack/void growth and tow/matrix interface degradation within the entire thickness of the composite. Whereas, at moderate thermal shock temperatures (i.e., 600 °C), high concentration of oxidation was observed at the surface of the composite. However, test specimens exposed to high thermal shock temperatures (i.e., above 600 °C) experienced both types of oxidation, i.e., surface degradation and oxidation within the exposed surfaces. Other effects of oxidation due to thermal shock on C/C composites were the rapid carbon matrix degradation (compared to that of the carbon fibers), "needle-shape" morphology at the exposed ends of the fibers and fiber breakage at the surface of the oxidized test specimens.

Furthermore, through-thickness compressive stiffness and strength decreased with increasing thermal shock peak temperature for test specimens exposed to one and three cycles. It can be concluded that the compressive stiffness of test specimens degraded approximately up to 55% for the most severe condition of three cycles of thermal shock with peak temperature of 1000 °C. Similarly, the compressive strength degraded about up to 17% for three cycles of thermal shock with peak temperature of 800 °C. Also, based on the stress–strain responses, it was concluded that non-linearity due to damage was induced to the material with increasing the number of cycles of the thermal shock conditions. Optical observations of the test specimens after one and three cycle thermal shock conditions showed that oxidation effects were significantly greater with increasing number of cycles of any thermal shock process, and even though both thermal configurations displayed similar oxidation behavior, lower values in the compressive properties of test specimens exposed to three thermal cycles were obtained.

Finally, it was suggested that tow/matrix debonding and interlayer shear failure were the main failure mechanisms of the 2D C/C composite specimens during compression tests, since high stress concentrations existed between the plies. Thus, it was concluded that 2D C/C composite properties were strongly affected by oxidation attack on carbon materials during thermal shock exposure in an oxidizing environment. This investigation is of great importance to decide the usability of C/C composites for high temperature structural applications.

Acknowledgments

The authors would like to thank The University of Texas at El Paso for their support through the University Research Initiative (URI) grant for the research presented in this paper.

References

[1] Manocha LM. High performance carbon–carbon composites. Sadhana 2003;28(1-2):349–58. http://dx.doi.org/10.1007/bf02717143.
[2] Zhao JX, Bradt RC, Walker Jr PL. Effect of air oxidation at 873 k on the mechanical properties of a carbon–carbon composite. Carbon 1985;23(1):9–13. http://dx.doi.org/10.1016/0008-6223(85)90189-7.
[3] Bacos M. Carbon–carbon composites, oxidation behavior and coatings protection. J Phys IV 1993;3(7):1895–903.
[4] Dhakate SR, Aoki T, Ogasawara T. High temperature tensile properties of 2d cross-ply carbon–carbon composites. Adv Mater Lett 2011;2:106.
[5] Sines G, Zheng Y, Vickers BD. Creep of carbon yarn and a carbon–carbon composite at high temperatures and high stresses. Carbon 1989;27(3):403–15. http://dx.doi.org/10.1016/0008-6223(89)90073.
[6] Hatta H, Kogo Y, Okura A. Research report for new energy and industrial technology development organization, NEDO-ITK-9209; 1993.
[7] Quenisset JM. Carbon combinations: Carbon-carbon composites. Adv Mater 1994;6(2):176–7. http://dx.doi.org/10.1002/adma.19940060222.
[8] Dillon F, Thomas KM, Marsh H. The influence of matrix microstructure on the mechanical properties of cfrc composites. Carbon 1993;31(8):1337–48. http://dx.doi.org/10.1016/0008-6223(93)90095-R.
[9] Fitzer E, Heym M. High temperatures-high pressures;1978. p. 10–29.
[10] Sato S, Kurumada A, Iwaki H, Komatsu Y. Tensile properties and fracture toughness of carbon-fiber felt reinforced carbon composites at high temperature. Carbon 1989;27(6):791–801. http://dx.doi.org/10.1016/0008-6223(89)90029-8.
[11] Through-thickness strain response of thick composites in compression, Research Center, Bethesda MD, Ship Materials Engineering Dept.
[12] DeTeresa SJ, Freeman DC, Groves SE. The effects of through-thickness compression on the interlaminar shear response of laminated fiber composites. J Compos Mater 2004;38(8):681–97.
[13] Attwood JP, Khaderi SN, Karthikeyan K, Fleck NA, OMasta MR, Wadley HNG, et al. The out-of-plane compressive response of composites. J Mech Phys Solids 2014;70(0):200–26. doi: http://dx.doi.org/10.1016/j.jmps.2014.05.017.
[14] McKee DW. Oxidation behavior and protection of carbon/carbon composites. Carbon 1987;25(4):551–7. http://dx.doi.org/10.1016/0008-6223(87)90197-7.
[15] Crocker P, McEnaney B. Oxidation and fracture of a woven 2d carbon–carbon composite. Carbon 1991;29(7):881–5. http://dx.doi.org/10.1016/0008-6223(91)90163-D.
[16] Shemet VZh, Pomytkin AP, Neshpor VS. High-temperature oxidation behaviour of carbon materials in air. Carbon 1993;31(1):1–6.
[17] Han JC, He XD, Du SY. Oxidation and ablation of 3d carbon–carbon composite at up to 3000 c. Carbon 1995;33(4):473–8.
[18] Glime WH, Cawley JD. Oxidation of carbon fibers and films in ceramic matrix composites: a weak link process. Carbon 1995;33(8):1053–60. http://dx.doi.org/10.1016/0008-6223(95)00034-B.
[19] Rodriguez MJ, Thrower PA, Radovic LR. On the oxidation resistance of carbon–carbon composites: importance of fiber structure for composite reactivity. Carbon 1995;33(4):545–54. http://dx.doi.org/10.1016/0008-6223(94)00180-8.
[20] Walker Jr PL, Rusinko Jr F, Austin LG. Gas reactions of carbon 1959; 11:133–221. doi: 10.1016/S0360-0564(08)60418-6.
[21] Luthra KL. Oxidation of carbon/carbon composites-a theoretical analysis. Carbon 1988;26(2):217–24. http://dx.doi.org/10.1016/0008-6223(88)90040-1.
[22] Lamouroux F, Bourrat X, Nasalain R, Sevely J. Structure/oxidation behavior relationship in the carbonaceous constituents of 2d-c/pyc/sic composites. Carbon 1993;31(8):1273–88. http://dx.doi.org/10.1016/0008-6223(93)90086-P.
[23] Thompson LF. Through-thickness compression testing and theory of carbon fibre composite materials. 2011.
[24] Shepheard B, Jackson D, Dixon M. Testing of thick carbon fiber laminate composites: comparison of thick with thin couple, current standards and product case study. National Physical Laboratory-Materials Centre.
[25] Lodeiro MJ, Broughton WR, Sims GD. Understanding limitations of through thickness test methods. Plast Rubber Compos 1999;28(9):416–24. http://dx.doi.org/10.1179/146580199101540583.
[26] Roy AK, Kim RY. Interlaminar normal stiffness and strength of thick orthotropic laminates: an experimental study. 1994; 13(10): 880–94. doi: 10.1177/073168449401301003.
[27] Tagarielli VL, Minisgallo G, McMillan AJ, Petrinic N. The response of a multi-directional composite laminate to through-thickness loading. Compos Sci Technol. 2010;70:1950–7. http://dx.doi.org/10.1016/j.compscitech.2010.07.013.
[28] Hodgkinson JM. Mechanical testing of advanced fibre composites. Elsevier; 2000.
[29] Park DC, Lee DG. Through-thickness compressive strength of carbon–phenolic woven composites. Compos Struct 2005;70(4):403–12.